A STATIC COMPRESSIVE STRENGTH MODEL FOR DAMAGED COMPOSITE LAMINATES

Andrew T. Rhead and Richard Butler

Department of Mechanical Engineering
University of Bath, Bath, BA2 7AY, UK.
R.Butler@bath.ac.uk

ABSTRACT

An analytical model for the prediction of compressive strength of composite structures with barely visible impact damage (BVID) is presented. The model represents the complex damage morphology using one of two simple methods based on circular approximations of the damage area and determines a critical interface for propagation of BVID. The finite strip program VICONOPT is used to calculate the strain at which thin-film buckling of the circular delaminated region occurs. The threshold strain is defined as the strain at which the strain energy release rate for the fracture of post-buckled delaminated plies along the delamination is equal to the critical Mode I value (G_{1C}) for the resin. Results obtained using the model are compared with experimental values for static strength of a variety of coupons and stiffened panels reported in the literature. For impacts on the skin under a stiffener the model is accurate to within 5% of the reported experimental result.

1. INTRODUCTION

The first generation of commercial aircraft that contain high proportions of composite parts such as the Airbus A350 and the Boeing 787 will enter service in the next few years. Hence, the need to advance understanding of the mechanics of composite structures has a renewed impetus. The approach to using composites in these new aircraft has been somewhat conservative which has meant the potential weight saving offered by the material may not have been completely realised. This approach has come about due to a variety of problems associated with incorporating composite materials into aircraft structures and their resistance to damage. This paper is aimed at the issue of damage and in particular, prediction of the static strength of compressively loaded composite components after barely visible impact damage (BVID) has occurred.

Currently, the effects of possible damage to composite structures are countered by employing empirically derived compressive strain limits. One of the contributory factors to conservativeness is the lack of modelling capability for determining the static strength of damaged laminates. Models available at present fall into two categories; FEA models such as [1] which are computationally expensive and require input of a predetermined layer of cohesive elements to model propagation of delamination, and analytical models [2, 3] which though computationally efficient, are relatively inaccurate and limited to isotropic or quasi-isotropic coupons.

This paper introduces an analytical model that is both efficient and that also produces results for structural features such as skin delamination beneath a stiffener. A quasi-static model that identifies the threshold strain, below which damage does not propagate, has been presented for fatigue problems in [4] and is extended here to predict static strength. Problems treated in this paper include; coupons tests from [5], [6] and [7], stiffened panels from [8], and new work carried out on a standard coupon, with stacking sequence optimised to maximise static strength.

2. ANALYTICAL MODEL

Previously [4], a quasi-static fatigue model based on the conditions apparent in the final stages of fatigue damage growth was presented, where delaminations at a significant depth within the sample are assumed to have buckled and subsequently opened. The model found the level of strain below which damage propagation did not occur, i.e. the threshold strain ε_{th}. The extension of this quasi-static fatigue model to static strength problems is dealt with in this paper.

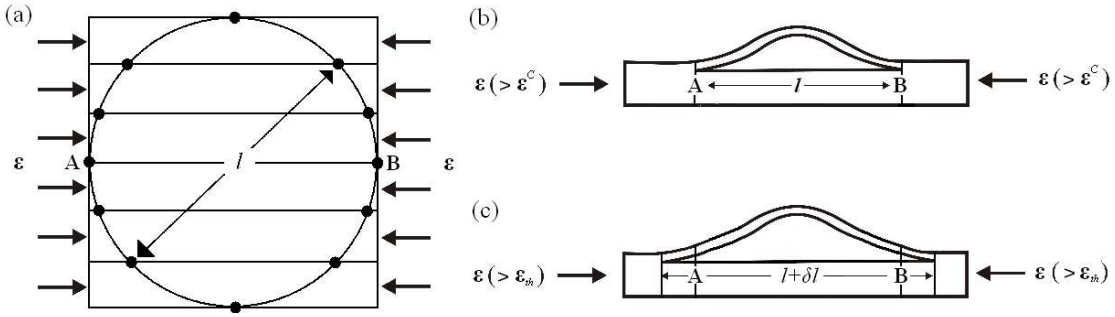

Figure 1: Thin film model showing (a) plan view of circular delaminated plate of diameter l with nodes and strips to illustrate VICONOPT discretisation, (b) post buckled central section through AB, (c) propagated central section.

A brief derivation of the model, including the key equations and concepts, is given here. Full derivations are available elsewhere [4]. The central concept of the derivation is to find the difference in energy in the post-buckled sublaminate before, Figure 1 (b), and after, Figure 1 (c), the growth of a delamination and to compare this difference to the Mode I fracture energy required to create a new unit of delamination. If sufficient energy is available then a new unit of delamination is created and propagation of the delamination will occur. Note that l is the length of the sublaminate immediately before propagation, and δl is an infinitesimal length associated with the length change due to propagation. As before, the model requires the calculation of the buckling strain ε^C of a delaminated circular region. Unlike the fatigue model where a single diameter l was used, in this case a range of different sized circular delaminations at various depths within the laminate are necessary to describe the initial conditions owing to the differing damage morphology assumed in static strength problems. These initial conditions will be discussed in Section 3.

The process of calculating ε^C is reliant on the composite buckling program VICONOPT [9-11]. In essence, the delaminated plate is modelled as a thin film such that the plate boundary along the circular perimeter of the delamination is assumed to be clamped. To obtain ε^C, VICONOPT uses the loadings placed on the thin film, by axial compression of the full laminate. The program models the plate as a series of finite strips, the edges of which are constrained by nodes approximating a circular boundary, see Figure 1(a). For the results presented later, 6 equal width strips were used with 12 constrained nodes at the junction of these strips and the circular boundary. Here, constrained implies that no buckling displacement or rotation is allowed at the nodes, thus approximating a fully clamped boundary. It should be noted that VICONOPT buckling analysis is fully general and can analyse the complex unbalanced and asymmetric sublaminates that can arise in the delaminated sublaminate [12].

The sublaminate, the thin buckled region in Figures 1 (b) and (c), is considered to contain bending energy and membrane energy. In order to calculate the energy due to bending it is assumed that the energy stored exactly equals the in-plane or stretching energy released [13]. Hence a combination of a simple work done equation and a comparison of buckling strains before and after propagation gives,

$$U_1(l) = A_{11}(\varepsilon - \varepsilon^C)\varepsilon^C \delta l \tag{1}$$

Note here that ε is the applied strain under displacement control and A_{11} is the axial stiffness of the sublaminate. Note also that the term $(\varepsilon - \varepsilon^C)$ implies bending energy is not stored in the sublaminate until after buckling has occurred.
The membrane energy associated with the sublaminate before and after buckling occurs is given by,

$$U_2(l) = \frac{A_{11}}{2} l[(\varepsilon^C)^2 + r(\varepsilon - \varepsilon^C)^2] \tag{2}$$

The amount of membrane energy stored by the sublaminate in the post-buckling regime is controlled by the choice of r, the ratio of post-buckled to pre-buckled stiffness of the sublaminate. Results obtained in [14] and [15] suggest that $0.35 < r < 0.65$ for orthotropic laminates. Previously, when the model was used for problems concerned with fatigue, $r = 0$ was chosen for simplicity. In this paper, for comparison, results for $r = 0.5$ are also given.
The above equations describe the energy available in the sublaminate prior to propagation. However, energy for propagation is also available in the form of membrane energy released from the section of the sublaminate of length δl which becomes delaminated during propagation. This energy is calculated using,

$$U_2^* = \frac{A_{11}}{2} \int_0^{\delta l} \varepsilon^2 dx \tag{3}$$

The bending and membrane energy in the sublaminate immediately after propagation occurs can be calculated by replacing l with $l + \delta l$ in Eqs. (1) and (2). Finally, it remains to compare energies before and after propagation to determine whether there is sufficient energy to cause propagation. Eq. (4) is employed to give this comparison at the instant propagation occurs. Here G_1 is the Mode I strain energy release rate (SERR).

$$G_1 = \lim_{\delta l \to 0} \{U_1(l) - U_1(l + \delta l) + U_2(l) - U_2(l + \delta l) + U_2^*\} \frac{1}{\delta l} \tag{4}$$

Hence

$$G_1 = \frac{A_{11}}{2}(\varepsilon - \varepsilon^C)[\varepsilon(1 - r) + \varepsilon^C(3 + r)] \tag{5}$$

By comparing this value to G_{1C}, the SERR required to cause Mode I failure of the resin, it is possible to determine whether propagation will occur for this level of strain. If the above equation is rearranged and G_1 is set equal to G_{1C} it is possible to calculate the threshold strain, when $\varepsilon = \varepsilon_{th}$, i.e.

$$\varepsilon_{th} = \frac{\varepsilon^C}{(1-r)}\left(-(1+r)+\sqrt{(1+r)^2+(1-r)\left((3+r)+\frac{2G_{1C}}{(\varepsilon^C)^2 A_{11}}\right)}\right) \tag{6}$$

The model is applied at each possible interface in turn up to a depth of 20% of the total thickness away from the face of the laminate. Hence the sublaminate at which the lowest threshold strain for propagation is determined will be the first to propagate. The remaining challenge in applying the model is to determine the size of the circular delaminations, which is the subject of the next section.

3. DAMAGE MORPHOLOGY

3.1 C-scan method

This method is based on images taken by C-scan that allow damage throughout the laminate thickness to be visualized. An image of the area of delamination is given at each interface where a circle that contains the full extent of the damage is assumed, see Figure 2(a). Thus the model is applied using each of these circles to represent the delamination in order to determine a threshold strain for each sublaminate. Note that, in each case the circular sublaminate is assumed to be fully intact, so that only one delamination is represented.

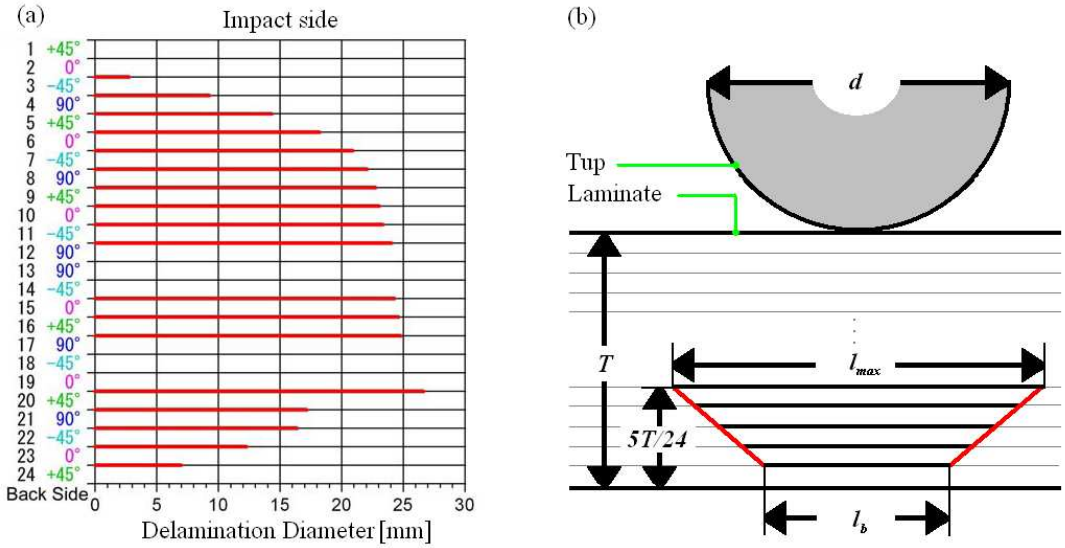

Figure 2: Damage morphology. (a) Sectional view of damage from [5] showing diameters of circles approximating through-thickness damage obtained from C-scan. (b) The linear damage model, tup impactor, and assumed delamination distribution over the lower 20% of laminate thickness.

There are a number of issues associated with determining damage circles this way. The first is the lack of available data in the literature giving through thickness C-scans. The second is that the resolution of C-scanning machines is not always sufficient to provide an accurate through thickness view of the damage. For example, in [6] the author states that the damage at interfaces 3 to 5 is indistinguishable. The

final issue is that in terms of future work it would be extremely time consuming to C-scan a large number of coupons or structural elements to determine these damage maps. This is compounded by the fact that the maps may be applicable to only that particular laminate (or even coupon, see [6]). This leads to the need for an alternative model.

3.2 Linear damage model

Figure 2(b) shows a linear damage model based on a distribution of circular delaminations reported by Uda and Ono [5], see Figure 2(a). Here, the diameter of circular delaminations in the lower 20% of the laminate thickness are approximated by assuming a linear decrease in diameter away from the largest delamination toward the back face of the laminate. A similar relationship can be inferred from Hull and Shi [14] who relate the formation of damage in this region of the laminate to bending of the laminate and peeling of the back face ply. Note that the critical delamination, the one at which damage propagates, is assumed to occur within the 20% of plies closest to the back face and hence only these plies are considered in the model. The delamination corresponding to the largest delamination $l_{\max}$, determined by a plan view C-scan (see Figure 3), is assumed to occur at 20% of laminate thickness T. Damage circles then decrease in diameter linearly so that the final diameter l_b corresponds to the delamination closest to the back face. It is assumed that this delamination is created by bending associated with the geometry of the tup, thus an empirical rule, based on [5] and Figure 2(a) is assumed whereby a tup of diameter 12mm causes an outer ply delamination of 7mm. Hence for the general case the delamination of diameter l_b closest to the back face, is determined using the formula

$$l_b = \frac{7d}{12} \tag{7}$$

Where d is the diameter of the tup used to impact the laminate.

3.3 Modelling of skin damage within a stiffened panel

The above is based on damage in coupons. In order to apply the model to the stiffened panels described in Section 4 some alterations are required. For impacts to the bay between stiffeners, where the laminate is the same thickness as the skin, the model can be applied as it is. For impacts to the panel underneath a stiffener foot (see Figure 4 (b)) Greenhalgh et al [8] found impacts caused damage throughout the skin and stiffener, hence it is assumed that the stiffener can be represented by a laminate of equal thickness and identical lay-up to the stiffener foot. In addition, assuming an impact on the skin surface, the circle of largest diameter is positioned closest to the impact face rather than the back face.

4. EXPERIMENTAL EXAMPLES

The model has been validated against a number of materials, the properties of which are given in Table 1, and various structural laminates, whose lay-ups are given in Table 2. The details of impact damage introduced into the coupons/stiffened panels are given in Table 3. All coupons and stiffened panels have been impacted to produce BVID and subsequently placed in axial compression to determine their static strength. The only exceptions to this are; the AS4/8552 (Optimised) coupon which has been impacted (see Figure 3) but is yet to be tested, and the AS4/8552 (Control) coupon

which is a theoretical comparison for the AS4/8552 (Optimised) coupon. For the control coupon, damage was based on the application of the linear damage model to the UT500/Epoxy (QI) data, which was also a 4mm thick quasi-isotropic laminate.

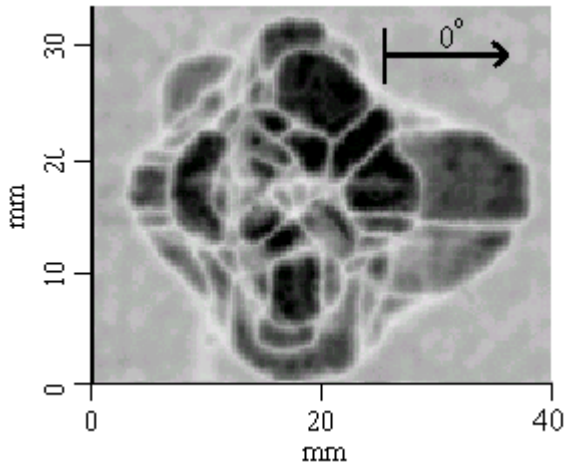

Figure 3: C-scan image showing the damage to an AS4/8552 (Optimised) coupon.

The HTA/6376 (ZD) and (QI) coupons from [6,7] had an anti-buckling guide applied leaving a 100mm x 100mm window. Note that because of the asymmetry of the HTA/6376 QI laminate it is necessary to establish impact and back faces in order to give the correct lay-up for the sublaminate involved in propagation. The UT500/Epoxy (QI) (Toho Tenax, QU135-197A) coupons from [5] were reduced from 50mm impacted width to 35mm width for compression testing, to allow for the capacity of the test machine. To prevent buckling of the UT500/Epoxy (QI) coupons, a gauge length of 35mm was chosen and the coupons were supported by guides along their longitudinal edges. The configurations of the stiffened panels from [8] and the locations of the impacts are given in Figure 4.

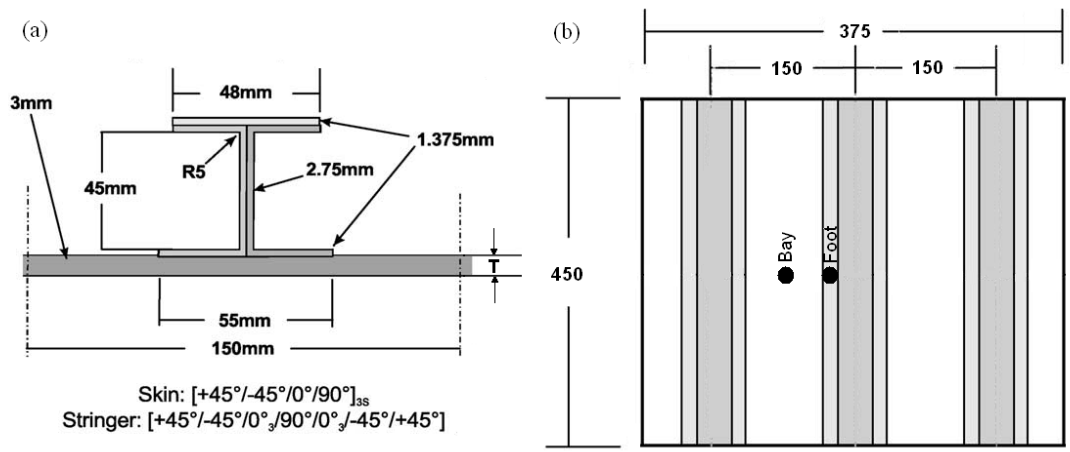

Figure 4: Stiffened panel example from [8]. (a) Stiffener configuration.(b) Plan view of panel showing impact sites.

Table 1
Material properties. t is layer thickness.

Material	E_{11} (GPa)	E_{22} (GPa)	G_{12} (GPa)	ν_{12}	t (mm)	G_{1C} (J/m^2)
UT500/Epoxy	124.0	9.6	5.75	0.344	0.167	280
HTA/6376	133.0	10.8	3.6	0.29	0.13/0.125	240
AS4/8552	128.0	10.3	6.0	0.3	0.125	261

Table 2
Example laminates showing relevant references in the literature.

Material	(Laminate ID)	Lay-up	Reference
UT500/Epoxy	(QI)	$[(45,0,-45,90)]_{3S}$	[5]
HTA/6376	(QI5)	$[(90,-45,45,0)_S,(0,45,-45,90)_S]_3$	[6]
HTA/6376	(QI14)	$[(90,-45,45,0)_S,(0,45,-45,90)_S]_3$	[6]
HTA/6376	(ZD)	$[45,-45,0,90,45,-45,0_2,(45,-45,0,90)_2,45,-45,0_2,45,-45,0,90]_S$	[6]
HTA/6376	(BAY)	$[45,-45,0,90]_{3S}$	[8]
HTA/6376	(FOOT)	$[45,-45,0,90]_{3S} + [45,-45,0_3,90,0_3,-45,45]$	[8]
AS4/8552	(Optimised)	$[(45,-45)_4,(90,0)_4]_S$	N/A
AS4/8552	(Control)	$[45,0,-45,90]_{4S}$	N/A

QI=Quasi-isotropic, ZD=Zero-dominated, BAY and FOOT give stiffened panel impact sites.

Table 3
Damage details for laminates of Table 2. T is laminate thickness and $l_{\max}$ is maximum damage diameter.

Material (Laminate ID)	T (mm)	Impact energy (J)	Tup diameter d (mm)	$l_{\max}$ (mm)
UT500/Epoxy (QI)	4	7.6	12	27
HTA/6376 (QI5)	6.24	27	7.5	52
HTA/6376 (QI14)	6.24	27	7.5	47
HTA/6376 (ZD)	6.24	27	7.5	49
HTA/6376 (BAY)	3	15	12.7	35
HTA/6376 (FOOT)	4.375	15	12.7	30
AS4/8552 (Optimised)	4	8	16	37
AS4/8552 (Control)	4	N/A	12	27

5. COMPARISON OF EXPERIMENTAL AND ANALYTICAL RESULTS

Analytical results are compared with experimental data in Table 4. These results indicate that, with the exceptions of the UT500/Epoxy (QI) and HTA/6376 (BAY) results, which will be discussed in Section 6, the linear damage approximation is within 16% (14% for $r = 0.5$) of the experimental values. Table 5 indicates the interface at which propagation takes place by providing the lay-up of the sublaminate for which growth first occurs as well as the associated buckling strain ε^C. The two damage prediction methods suggest growth at different interfaces and so sublaminate lay-ups for the critical interfaces are given according to each method. Failure occurs for the HTA/6376 (BAY) stiffened panel at 5830 μstrain. Note that for the result HTA/6376 (FOOT) propagation first occurs at an experimental strain of 4300 μstrain. Results for the AS4/8552 (optimised) and (control) coupons are currently limited to

analysis only. The principle for optimization was based on two factors; increasing the delaminated plate buckling strain and reducing the SERR. The former was achieved by putting all the $\pm 45^o$ layers to the outer faces of the laminate, thus increasing buckling resistance. The latter was achieved by moving all the 0^o fibres to the central region as these fibres tend to cause strain energy to release earlier. The optimised coupon result is based on the damage pattern recorded in an impact test of an optimised coupon (see Figure 3) but, as yet, no experimental failure strain is available.

Table 4
Experimental failure strains and analytical threshold strains for laminates described in Section 4. r is post-buckled stiffness ratio, see Eq. (2).

Material (Laminate ID)	Experimental failure strain (μstrain)	Analytical threshold strain (μstrain) C-scan method r=0	C-scan method r=0.5	Linear model r=0	Linear model r=0.5
UT500/Epoxy (QI)	5277†	4198	4330	4074	4144
HTA/6376 (QI14)	5025	3474	3682	4382	4496
HTA/6376 (QI5)	5025	3985	4334	4248	4350
HTA/6376 (ZD)	4439	4132	4171	4542	4588
HTA/6376 (FOOT)	4461	N/A	N/A	4219	4296
HTA/6376 (BAY)	3550-4810*	N/A	N/A	3659	3957
AS4/8552 (Optimised)	N/A	N/A	N/A	4997	5024
AS4/8552 (Control)	N/A	N/A	N/A	4176	4295

†Boundary conditions delay failure, see section 6.
*propagation of damage rather than failure occurs between these values.

Table 5
Lay-ups and associated VICONOPT buckling strains for critical sublaminates giving analytical results of Table 4.

Material (Laminate ID)	C-scan method Lay-up	C-scan method Buckling strain (μstrain)	Linear model Lay-up	Linear model Buckling strain (μstrain)
UT500/Epoxy (QI)	[45,0]	2446	[45,0,-45]	2764
HTA/6376 (QI14)	[90,90,-45,45,0]	1608	[45,0]	2690
HTA/6376 (QI5)	[45,0]	1517	[45,0]*	2416*
HTA/6376 (ZD)	[45,90,0,-45,45]	3113	[0,45,-45]	3381
HTA/6376 (BAY)	N/A	N/A	[0,-45,45]	1422
HTA/6376 (FOOT)	N/A	N/A	[0,-45,45]†	2822†
AS4/8552 (Optimised)	N/A	N/A	$[45,-45]_3$	4037
AS4/8552 (Control)	N/A	N/A	[45,0,-45]	2504

*Results for r=0.5 are [-45,45,0], 3008 (μstrain). † Results for r=0.5 are [90,0,-45,45], 2236 (μstrain).

6. DISCUSSION

The model provides a good approximation of failure/propagation strain for a wide range of materials and structural features with varying laminate thickness and damage geometry. In general, the threshold strains calculated using the linear damage model give better agreement with experimental failure strain than the C-scan method. In particular, the linear model predicts similar threshold strains for identical coupons (HTA/6376 (QI14) and (QI5)) where the variation of damage shown on through-thickness C-scans means the C-scan method gives variable results.

With the exception of the analytical strain for HTA/6376 (ZD), the threshold strains obtained using the linear damage model are lower than the experimental failure strain. Failure generally occurs when damage propagates to the edge of the coupon and not at the threshold strain, which gives initial propagation. In comparison, a similar rationale can be applied to stiffened panels where the prevalent failure mechanism is stiffener detachment. Hence damage in the bay needs to propagate under the stiffener to cause detachment and requires a higher strain to cause failure than damage under the stiffener foot where propagation causes immediate partial detachment. This is reinforced by the results. For bay impact, HTA/6376 (BAY), the threshold strain is predicted correctly but the failure strain of 5830 μstrain is significantly higher, whereas for the HTA/6376 (FOOT) failure (4461 μstrain) quickly follows propagation (4300 μstrain) which is accurately predicted.

The UT500/Epoxy (QI) result is influenced by experimental boundary conditions. The $l_{\max}$ damage diameter for this coupon is 27mm in an exposed square of laminate 35mm in width and length. Outside this area the coupon is clamped at its ends and supports run along its unclamped edges to prevent buckling. This proximity of supports may well delay failure of the coupon and is thought to explain the poor comparison with the analytical results for this problem.

For HTA/6376 (QI5), using a value of $r = 0.5$ gives a more favourable comparison of analytical and experimental threshold strains than $r = 0$. Otherwise, $r = 0$ is sufficient.

The depth of failure interface is predicted by the model, see Table 5. Only Greenhalgh et al [8] recorded the experimental depth of the critical delamination and then only for the foot impact (HTA/6376 (FOOT)). In this case the critical interface was between the third and fourth plies which is in agreement with the model.

Finally, the AS4/8552 (Optimised) and (Control) results show that the optimised coupon has an increased static strength compared to the control coupon. For the linear damage model with $r = 0$ the static strength of the optimised coupon is approximately 120% of the control coupon. For $r = 0.5$ the value is 117%. Note that the control coupon has a significantly smaller damage envelope than the optimised coupon and so the predicted increases may well be conservative.

7. CONCLUSIONS AND FUTURE WORK

When applied in conjunction with a simple linear representation of damage the analytical model is accurate to within 16% of experimental values for static strength in a variety of materials and structural types with realistic boundary conditions. Results from [8] indicate that impacts under the stiffener foot of a stiffened panel are more serious than those to the bay i.e. the reduction in strength associated with impacts under the stiffener foot is much greater than that attributed to bay impacts. Hence modelling of the former problem is more important and here the model gives an accurate, slightly conservative result. An optimised coupon is expected to achieve a 20% gain in static strength in comparison to a control coupon.

In future the model will be applied to bending rather than compression of panels and to investigate the stability of damage growth in order to determine the connection between threshold and failure strains. An analytical approach to determining the largest delamination diameter, together with an improved representation of damage morphology would also be beneficial. Finally, a series of experimental tests are planned to validate the threshold strain predicted for the optimised coupon.

ACKNOWLEDGEMENTS

Andrew Rhead is sponsored by the Great Western Research (GWR) alliance and Airbus UK. The authors are grateful to the University of Bristol who provided assistance with the AS4/8552 coupon and acknowledge the contributions made to this paper by Moustafa Kinawy and Neil Baker at the University of Bath.

REFERENCES

1- Nilsson K.-F., Asp L.E., Alpman J.E, Nystedt L., "Delamination buckling and growth for delaminations at different depths in a slender composite panel". *Int.J. Solids and Structures*, 2001;38:3039-3071.

2- Kardomateas G.A.,"The initial post-buckling and growth behaviour of internal delaminations in composite plates", *Journal of Applied Mechanics*, 1993;60:903-910.

3- Chai H., Babcock C.D., "Two-dimensional modelling of compressive failure in delaminated laminates", *Journal of Composite Materials*, 1985;19:67-98.

4- Rhead, A.T., Butler, R., Hunt, G.W., "Post-buckled propagation model for compressive fatigue of impact damaged laminates", *International Journal of Solids and Structures* 2008, doi: 10.1016/j.ijsolstr. 2008.03.014 (in press). http://dx.doi.org/10.1016/j.ijsolstr.2008.03.014.

5- Uda N., Ono K., "Compression fatigue failure of CFRP laminates with impact damage", *Proceedings of 16th ICCM Kyoto, Japan*, 2007.

6- Melin G.L., Schön J., "Buckling behaviour and delamination growth in impacted composite specimens under fatigue load: an experimental study" *Composites Science and Technology*, 2001;61:1841-1852.

7- Melin G.L., Schön J., Nyman T., "Fatigue testing and buckling characteristics of impacted composite specimens", *Int J Fatigue,* 2002; 24: 263-272.

8- Greenhalgh E., Meeks C., Clarke A., Thatcher J., "The effect of defects on the performance of post-buckled CFRP stringer-stiffened panels", *Composites: Part A*, 2003;34:623-633.

9- Williams F.W., Anderson M.S., Kennedy D., Butler R., Aston G., 1990. *User manual for VICONOPT. NASA* CR-181966.

10- Wittrick W.H., Williams F.W., "Buckling and vibration of anisotropic or isotropic plate assemblies under combined loadings" *Int. J. Mech. Sci*., 1973;16:209-239.

11- Anderson M.S., Williams F.W., Wright C.J., "Buckling and vibration of any prismatic assembly of shear and compression loaded anisotropic plates with an arbitrary supporting structure" *Int. J. Mech. Sci.,* 1982;25(8):585-596.

12- Anderson M.S., Kennedy D., "Transverse shear deformation in exact buckling and vibration of composite plate assemblies", *AIAA J*, 1993;31(10):1963-1965.

13- Thompson J.M.T., Hunt G.W., "Elastic Instability Phenomena" 1st edition, *Wiley and Sons*, 1984.

14- Koiter W.T., Pignataro M., "A general theory for the interaction between local and overall buckling of stiffened panels" *Delft University of Technology Report,* WTHD-83, 1976.

15- Weaver P.M., Diaconu C.G., "Approximate solution and optimum design of compression-loaded, postbuckled laminated composite plates", *AIAA J,* 2005;43(4):906-914.

16- Hull D., Shi Y., "Damage mechanism characterization in composite damage tolerance investigations", *Composite Structures*, 1993;23:99-120.